11B.3 THE WATER BUDGET OF TYPHOON NARI (2001) AT LANDFALL

Ming-Jen Yang*[1], Scott A. Braun[2], and Den-Shun Chen[1]
[1]National Central University, Chung-Li, Taiwan
[2]NASA/Goddard Space Flight Center, Greenbelt, Maryland, USA

1. INTRODUCTION

Typhoon Nari struck Taiwan on September 16, 2001; it brought heavy rainfall (with three-day-total rainfall of more than 1400 mm), strong wind gusts, fresh flood, and caused severe economical and societal damage, including 92 human lives (Sui et al. 2002). Because of the tremendous rainfall and severe disaster produced by Nari, there are several studies on Nari from both observational and modeling aspects. For example, precipitation efficiency of Typhoon Nari over the ocean was discussed in Sui et al. (2005); the flooding simulation of Nari was examined in Li et al. (2005); and Yang (2008) investigated the essential microphysical processes of Typhoon Nari (2001) at landfall. Yang et al. (2008; hereafter referred to as Part I) conducted a quadruply nested-grid MM5 model simulation with the finest grid size of 2 km for Nari and showed that the model reproduces reasonably well the kinematic and precipitation features as well as the structural changes of Nari, as verified against radar and rain-gauge observations. These include the storm track, contraction and sizes of the eye and eyewall, the spiral rainbands, the rapid pressure rise (~1.67 hPa h^{-1}) during landfall, and the nearly constant intensity after landfall. In addition, the model captures the horizontal rainfall distribution and some local rainfall maxima associated with Taiwan's orography.

In order to further understand the evolution of clouds and precipitation of Typhoon Nari upon its landfall on Taiwan, water budgets for vapor, cloud, and precipitation of Nari are conducted in this study by analyzing the MM5 model outputs from Part I with high spatial and temporal resolutions (2-km horizontal grid size and 2-min output interval). The first objective of this study is to investigate the evolution of water vapor, cloud, and precipitation of Nari during its landfall on Taiwan, especially for the transition from the more axisymmetric structure over the ocean to the highly-asymmetric features over mountains. The second objective is to understand what portions of heavy rainfall of Nari were produced *in-situ*, i.e., locally generated, and what potions of rainfall were produced by precipitation transported remotely from the surrounding moisture-rich ocean area. The third purpose is to examine whether the precipitation efficiency is indeed increased after Nari's landfall on the mountainous island of Taiwan. Through the analyses of water vapor, cloud, and precipitation budgets, we wish to gain physical insights into how vapor, clouds, and precipitation are generated within Nari and how microphysical processes are modified as Nari encountered the mountainous topography on Taiwan.

*Corresponding author address: Prof. Ming-Jen Yang, Department of Atmospheric Sciences, National Central University, Chung-Li, 320, Taiwan. E-mail: mingjen@cc.ncu.edu.tw

2. METHODOLOGY

All water budget calculations are based on the governing equations used in the PSU-NCAR MM5 model (Dudhia 1993; Grell et al. 1995). Following Liu et al. (1999), Zhang et al. (2000; 2001), and Braun (2006), because of the quasi-axisymmetric nature of TCs, we will discuss the water budgets of Nari in the cylindrical coordinate (r, λ, z), where r is the radius from the TC center pointing outward, λ is the azimuthal angle, and z is the vertical height axis. While Nari is over ocean, the TC center is defined as the center of minimum sea-level pressure; while Nari is over Taiwan island, the TC center is defined as the primary vortex circulation center.

As in Braun (2006), the governing equation for water vapor in a TC-following framework can be written as

$$\frac{\partial q_v}{\partial t} = -\nabla \cdot (q_v \mathbf{V}') - \frac{\partial (q_v w)}{\partial z} + q_v \left(\nabla \cdot \mathbf{V}' + \frac{\partial w}{\partial z}\right), \quad (1)$$
$$- C + E + B_v + D_v$$

the equation for cloud can be written as

$$\frac{\partial q_c}{\partial t} = -\nabla \cdot (q_c \mathbf{V}') - \frac{\partial (q_c w)}{\partial z} + q_c \left(\nabla \cdot \mathbf{V}' + \frac{\partial w}{\partial z}\right), \quad (2)$$
$$+ Q_{c+} - Q_{c-} + B_c + D_c$$

and the equation for precipitation can be written as

$$\frac{\partial q_p}{\partial t} = -\nabla \cdot (q_p \mathbf{V}') - \frac{\partial (q_p w)}{\partial z} + q_p \left(\nabla \cdot \mathbf{V}' + \frac{\partial w}{\partial z}\right), \quad (3)$$
$$+ \frac{\partial (q_p V_T)}{\partial z} + Q_{p+} - Q_{p-} + D_p$$

where q_v, q_c, q_p are the water vapor, cloud (cloud ice

and cloud water), and precipitation (rain, snow, and graupel) mixing ratios; $\mathbf{V}'$ is the storm-relative horizontal air motion; w and V_T are the vertical air and hydrometeor terminal velocities; Q_{c+}, Q_{c-}, Q_{p+}, and Q_{p-} are the cloud and precipitation microphysical source (+) and sink (–) terms; *C* is the condensation and deposition; *E* is the evaporation and sublimation; $C - E = Q_{c+} - Q_{c-} + Q_{p+} - Q_{p-}$; B_v and B_c are the contributions from the planetary boundary layer parameterization to the vapor and cloud budgets; D_v, D_c, and D_p are parameterized turbulent diffusion terms for vapor, cloud, and precipitation, respectively. Microphysical source and sink terms are directly output from Reisner et al. (1998) parameterization. Note that the artificial source terms associated with setting negative mixing ratios (caused by numerical errors associated with the finite-differencing treatment of the advection terms) to zero, which are discussed in Braun (2006), are not included in this study. The first two terms on the right-hand sides of Eqs. (1)–(3) are the horizontal and vertical flux divergence terms, so a flux convergence (divergence) gives a positive (negative) change in the respective mixing ratio field. The third term on the right-hand side of Eqs. (1)–(3) is the change in the mixing ratio field due to the three-dimensional airflow divergence following the storm motion. Each term in Eqs. (1)–(3) is directly output from the MM5 model except for the storm motion contribution, which is calculated offline. Parameter name and mathematical formulation of each budget term is given in Table 1.

While performing the water-budget calculations, several definitions of averages are used. First, the temporal and azimuthal mean is defined as

$$\overline{[]} = \frac{1}{2\pi(T_2 - T_1)} \int_{T_1}^{T_2} \int_0^{2\pi} \rho[] \partial\lambda \partial t \,, \qquad (4)$$

the time-averaged and vertically integrated amount is

$$[\wedge] = \frac{1}{(T_2 - T_1)} \int_{T_1}^{T_2} \int_{Z_B}^{Z_T} \rho[] \partial z \partial t \,, \qquad (5)$$

and the time-averaged, volumetrically integrated amount is defined as

$$\overline{\overline{[]}} = \int_{Z_B}^{Z_T} \int_{R_1}^{R_2} \overline{[]} 2\pi r \partial r \partial z \,, \qquad (6)$$

where T_1 and T_2 are the beginning and ending times for the analysis (13 h and 14 h while Nari is over ocean); Z_B and Z_T are the heights of the lowest and uppermost half-σ levels of the model domain; and R_1 and R_2 are the radial limits of integration. The typhoon circulation of Nari over ocean can be separated by two distinct components: the inner core (*R* = 0–50 km) including the eye and eyewall, and outer rainband (*R* = 50–150 km) region including the rain bands and stratiform precipitation (see Fig. 1). Thus R_1 and R_2 are 50 km and 150 km, respectively, while Nari is over the ocean for the simulation time period of 13–14 h.

The units of the quantities derived from Eqs. (4)–(6) are kg m^{-3} h^{-1}, kg m^{-2} h^{-1}, and kg h^{-1}, respectively. Each water budget term in Eqs. (1)–(3) is averaged using Eq. (6) from *R* = 0 (eye) to *R* = 50 km for the inner-core region, and from *R* = 50 km to *R* = 150 km for the outer rainband region. All values are then normalized by the total condensation between *R* = 0 to *R* = 150 km and then multiplied by 100. All calculated budget terms (with definitions given in Table 1) are shown in Fig. 5.

3. RESULTS

Figure 1a shows the horizontal distribution of the radar reflectivity composite on the 2-km grid using the 1-h (13–14 h) temporally averaged simulation result of Typhoon Nari, and a further zoom-in picture is shown in Fig. 1b. It is clear in Fig. 1b that while Nari is over ocean, it has the highly axisymmetric precipitation structure with a clear eye, eyewall, connecting rainband, and a principal rainband. If we take a vertical cross section along Line AB (in cross-track direction), strong radar echo occurs in the eyewall with a outward-tilted vertical axis, and several rainbands are radially 20–50 km behind the eyewall (Fig. 1c).

The volume integrals of the one-hourly averaged microphysical source terms of evaporation (plus sublimation) and condensation (plus deposition) are shown in Figs. 2a and 2b, respectively.

Evaporation of falling raindrops and small cloud droplets, along with sublimation of ice crystals in cloud anvils, occur over a much wider area (Fig. 2a). In contrast, intense condensation occurs in a more compact region within the eyewall, and less intense condensation and deposition are located in the spiral rain bands (Fig. 2b).

Figure 3 shows the vertical cross section with evident asymmetric precipitation and kinematics structures in the cross-track direction (along Line AB). Deep updrafts with maximum intensity about 1.4 m s^{-1} (after one-hour average) occur within the evident outward-sloping eyewall on the northwest side; on the other hand, updrafts on the southeast eyewall are relatively weaker (Figs. 3a, b). Weak convective updrafts can be found in the upper levels in the outer rainband and stratiform precipitation region. Abundant supercooled liquid dropets are found at the low-to-mid levels within the eyewall (Fig. 3b). Intense radial inflows are in the low level (peaked at –18 m s^{-1} below the marine PBL), and radial outflows are found at mid-to-upper levels.

Figure 4 illustrates the azimuthally and 1-h (13–14 h) temporally averaged water budget terms of Nari calculated following the definition given in Eq. (4). Large amount of cloud condensation occurs within the eyewall, and less amount of cloud condensation is found in the outer rain-band and stratiform precipitation region; vapor deposition also occurs in the outer region, although its magnitude is much less than the condensation rate (Fig. 4a). Large amount of evaporation by raindrops and cloud droplets are produced in the inner core, and a less degree of evaporation and sublimation is found in outer region (Fig. 4b). Convergence of water vapor by storm-relative airflow occurs within most of the storm (especially within the eyewall), while divergence of water vapor is only found at low level (Fig. 4c). Similarly, convergence of total water condensate (including liquid and ice phases) occurs within the entire storm (Fig. 4d). Rain fallout term generates heavy rainfall inside the eyewall, which is largely produced by melting of graupel particles, and also some rainfall associated with melting of snowflakes in outer region (Fig. 4e). As shown in Braun (2006), the horizontal flux divergence and vertical flux divergence of water vapor are largely out of phase, and they are mainly produced below 5 km (Figs. 4f and 4g). Similarly, the horizontal flux divergence and vertical flux divergence of total condensate are also largely out of phase, but they can be found at mid-to-upper levels (Figs. 4h and 4i).

Figure 5 shows that the inward-to-eyewall horizontal vapor transport within the PBL is about 21% of total condensation and the PBL source term is only about 1.4% of total condensation. This indicates that the ocean source of water vapor in the inner core region is a small portion of horizontal transport, consistent with the finding of Braun (2006). The microphysical precipitation efficiency, which is defined as the volume-integral precipitation divided by the volume-integral condensation and deposition, in the inner core region is about 72% (23.2/32.4) in the inner core, is about 57% (38.5/67.6) in outer rainband region.

Figure 6 displays the corresponding volume integrals of the one-hourly (23–24 h) averaged microphysical source terms of evaporation (plus sublimation) and condensation (plus deposition) after Nari's landfall over northern Taiwan. It is evident in Fig. 6 that both evaporation and condensation rates are more intense and locally located as the strong rotating air flows over the rugged peaks and valleys within the Central Mountain Range on Taiwan. More details of the terrain-induced asymmetries on Nari's microphysical fields and water budget terms will be given during the oral presentation at the conference.

Reference

Braun, S. A.: 2006: High-Resolution Simulation of Hurricane Bonnie (1998). Part II: Water Budget. *J. Atmos. Sci.*, **63**, 43–64.

Dudhia, J. 1993: A nonhydrostatic version of the Penn State/NCAR mesoscale model: Validation tests and simulation of an Atlantic cyclone and cold front. *Mon. Wea. Rev.*, **121**, 1493–1513.

Grell, G. A., J. Dudhia, and D. R. Stauffer, 1995: A description of the fifth-generation Penn State/NCAR Mesoscale Model. NCAR Technical Note, 138 pp.

Li, M.-H., M.-J. Yang, R. Soong, and H.-L. Huang**,** 2005: Simulating typhoon floods with gauge data and mesoscale modeled rainfall in a mountainous watershed. *J. Hydrometeor*., **6**, 306–323.

Liu, Y., D.-L. Zhang, and M. K. Yau, 1999: A multiscale numerical study of Hurricane Andrew (1992). Part II: Kinematics and inner-core structures. *Mon. Wea. Rev.*, **127**, 2597–2616.

Reisner, J., R. J. Rasmussen, and R. T. Bruitjes, 1998: Explicit forecasting of supercooled liquid water in winter storms using the MM5 mesoscaled model. *Quart. J. Roy. Meteor. Soc*., **124**, 1071–1107.

Sui, C.-H., and Co-authors, 2002: Typhoon Nari and Taipei flood—A pilot meteorology-hydrology study. EOS, Transctions, *Amer. Geophy. Union*, **83**, 265, 268–270.

Sui, C.-H., X. Li, M.-J. Yang, and H.-L. Huang**,** 2005: Estimation of oceanic precipitation efficiency in cloud models. *J. Atmos. Sci.*, **62**, 4358–4370.

Yang, M.-J., 2008: Microphysical processes of Typhoon Nari (2001) at landfall. *Preprints, The 28th Conference on Hurricane and Tropical Meteorology*, Orlando, FL, 28 April to 2 May 2008, Amer. Meteor.

Soc., 12C.5.

Yang, M.-J., D.-L. Zhang, and H.-L. Huang, 2008: A modeling study of Typhoon Nari (2001) at landfall. Part I: The topographic effects. *J. Atmos. Sci.*, **65**, 3095-3115.

Zhang, D.-L., Y. Liu, and M. K. Yau, 2000: A multiscale numerical study of hurricane Andrew (1992). Part III: Dynamically induced vertical motion. *Mon. Wea. Rev.*, **128**, 3772–3788.

Zhang, D.-L., Y. Liu, and M. K. Yau, 2001: A multiscale numerical study of Hurricane Andrew (1992). Part IV: Unbalanced Flows. *Mon. Wea. Rev.*, **129**, 92–107.

Table 1. Water budget parameter names.

Name	Term	Description/comment
Cond	$\overline{\overline{C}}$	Condensation + deposition
Evap	$\overline{\overline{E}}$	Evaporation + sublimation
VF	$-\overline{\overline{\frac{\partial(q_x w)}{\partial z}}}$	Vertical flux, typically negligible since w ~ 0 at Z_s and Z_t
HFP	$\overline{\overline{-\nabla\cdot(q_x\mathbf{V}')}} > 0$	Inward-directed (positive) horizontal flux convergence
HFN	$\overline{\overline{-\nabla\cdot(q_x\mathbf{V}')}} < 0$	Outward-directed (negative) horizontal flux convergence
Div	$\overline{\overline{q_x\left(\nabla\cdot\mathbf{V}'+\frac{\partial w}{\partial z}\right)}}$	Divergence term
P	$\overline{\overline{\frac{\partial(q_p V_T)}{\partial z}}}$	Surface precipitation flux
Diff	$\overline{\overline{D_x}}$	Numerical diffusion
PBL	$\overline{\overline{B_x}}$	Boundary layer source
Tend	$\overline{\overline{\frac{\partial q_x}{\partial t}}}$	Storage term

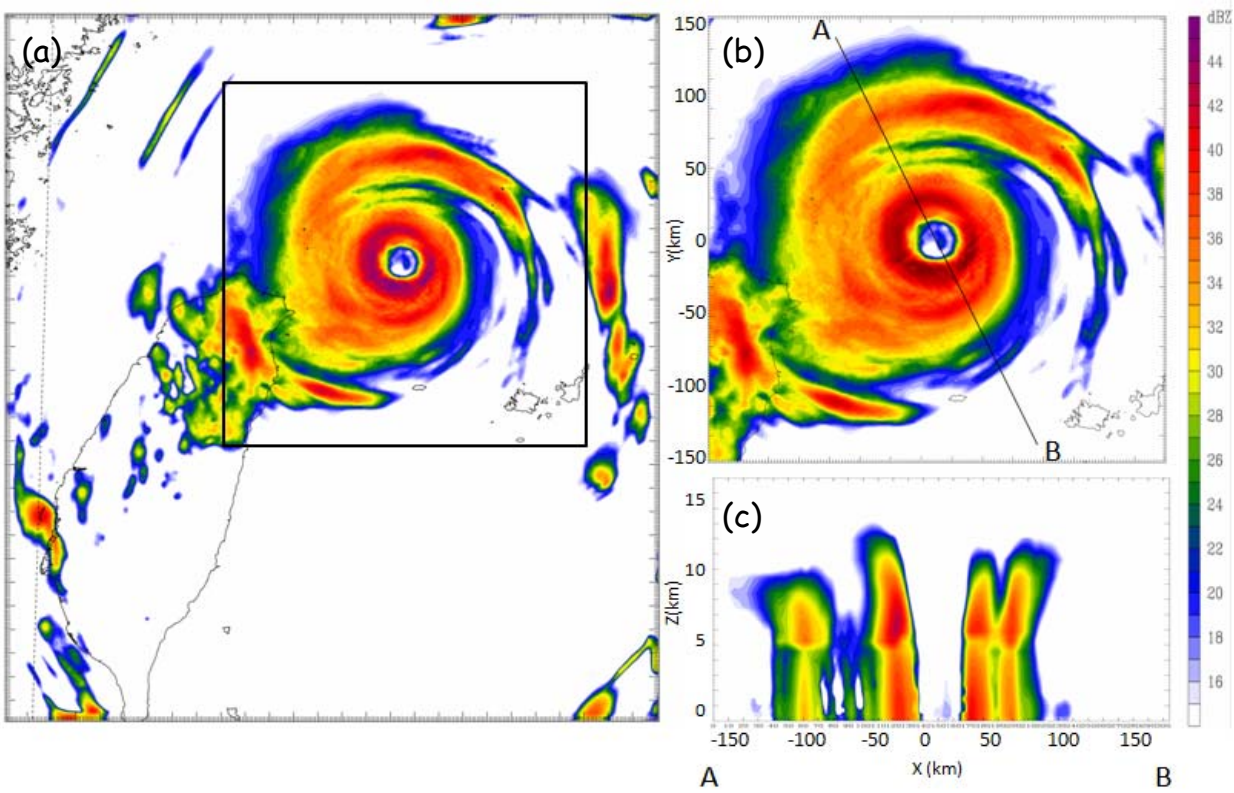

Figure 1: Vertical-maximum composite of one-hour averaged radar reflectivity (in units of dBZ) of Typhoon Nari during 01–02 UTC 16 Sept 2001 on (a) the 2-km grid and (b) the 300 km x 300 km square whose horizontal area is shown by the bold square in (a). Vertical cross section in (c) is the one-hour averaged radar reflectivity along Line AB whose horizontal position is shown in (b).

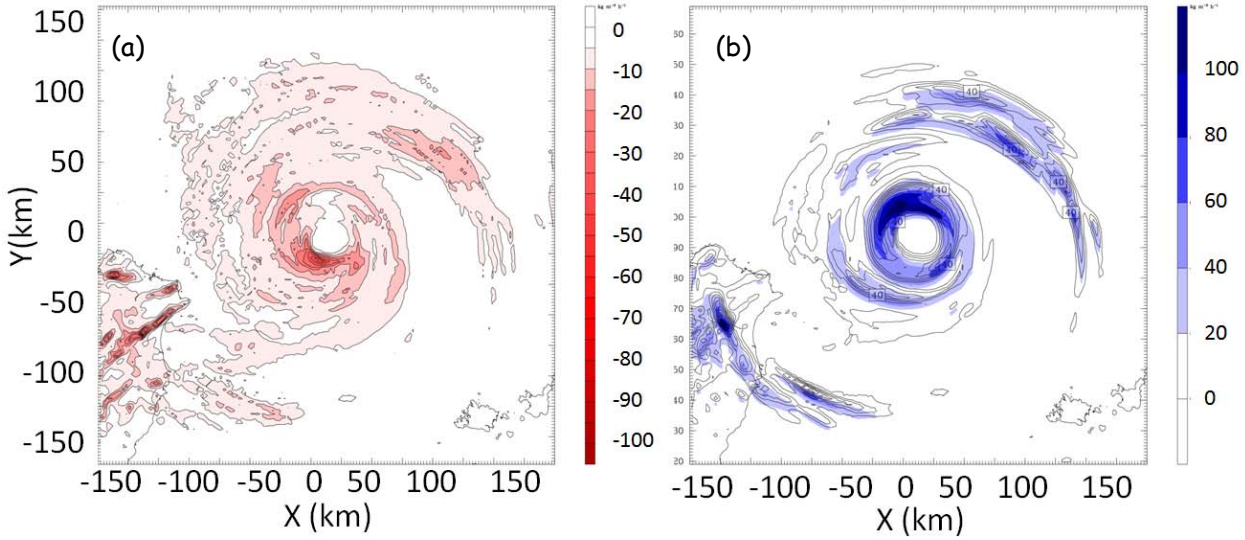

Figure 2: Volume integral of one-hour (13–14 h) temporal averaged microphysical source terms of (a) evaporation and (b) condensation. Contour intervals are 5 kg m^{-2} h^{-1} in (a) and 10 kg m^{-2} h^{-1}in (b).

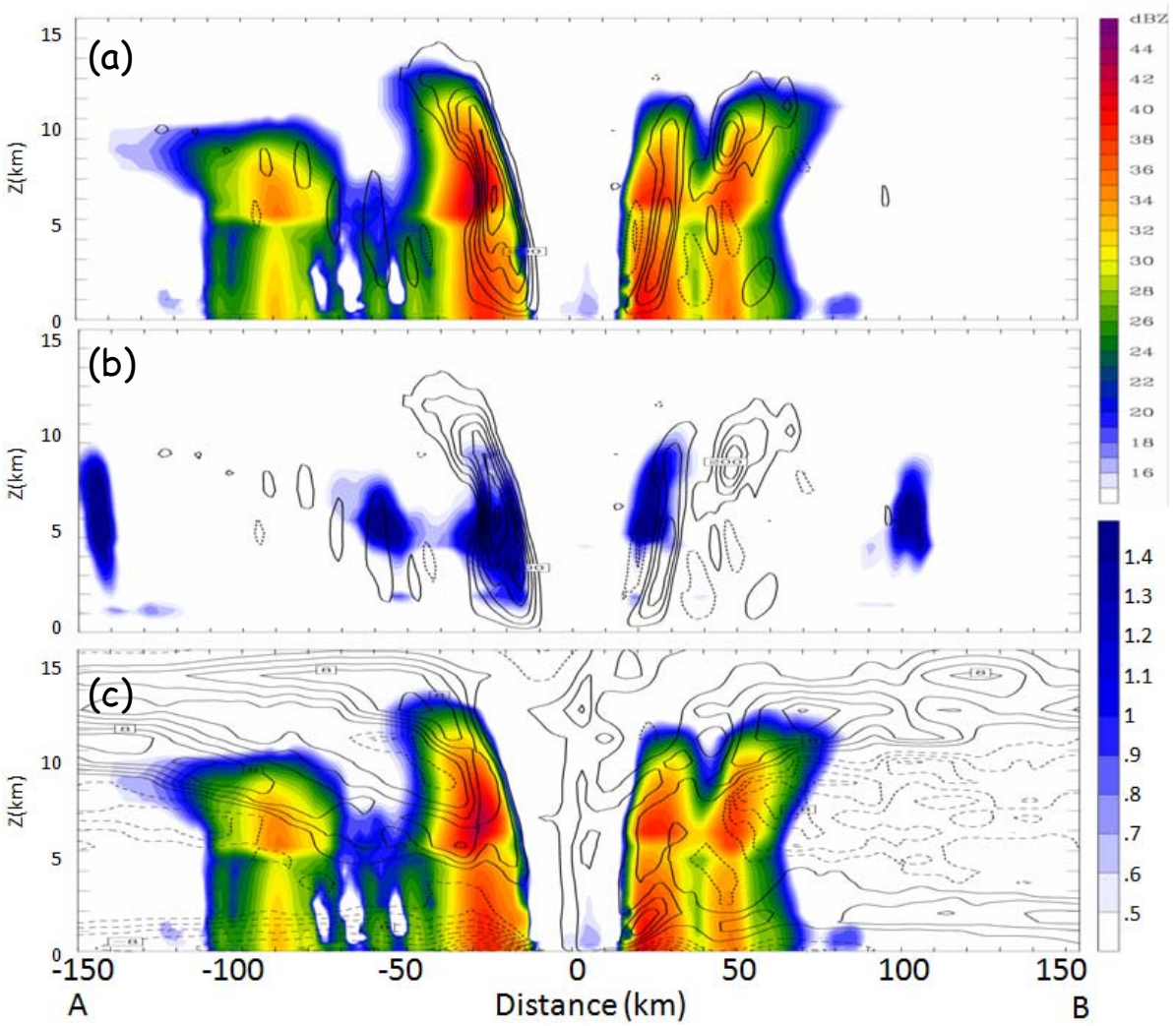

Figure 3: Vertical cross section of (a) radar reflectivity (in dBZ; colored) and vertical velocity (in cm s^{-1}; positive value is solid-contoured and negative value is dashed-contoured), (b) total cloud (cloud ice and cloud water) mixing ratio (in g kg^{-1}; blue shaded) and vertical velocity (in cm s^{-1}; positive value is solid-contoured and negative value is dashed-contoured), and (c) radar reflectivity (in dBZ; colored) and storm-relative radial velocity (in m s^{-1}; positive value is solid-contoured and negative value is dashed-contoured) taken along Line AB from the 2-km simulation result averaged at *t* = 13–14 h or 0100–0200 UTC 16 Sept 2001.

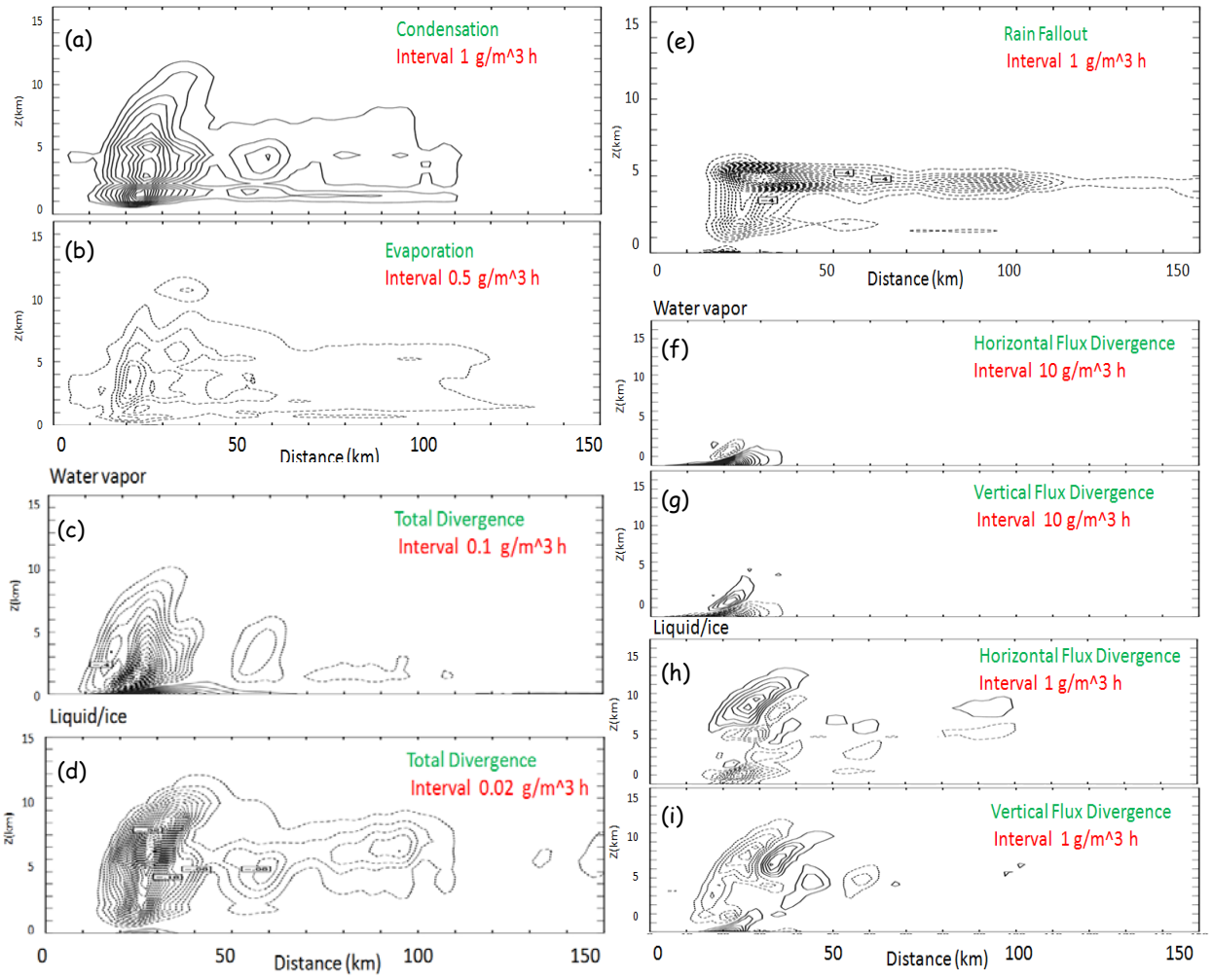

Figure 4: Azimuthally and one-hour (13–14 h) temporally averaged water budget terms (in units of g m^{-3} h^{-1}) of Typhoon Nari over the ocean: (a) condensation plus deposition, (b) evaporation plus sublimation, (c) water vapor divergence, (d) total condensate (liquid and ice phases) divergence, (e) rain fallout, (f) horizontal flux divergence for water vapor, (g) vertical flux divergence for water vapor, (g) horizontal flux divergence for total condensate, and (h) vertical flux divergence for total condensate.

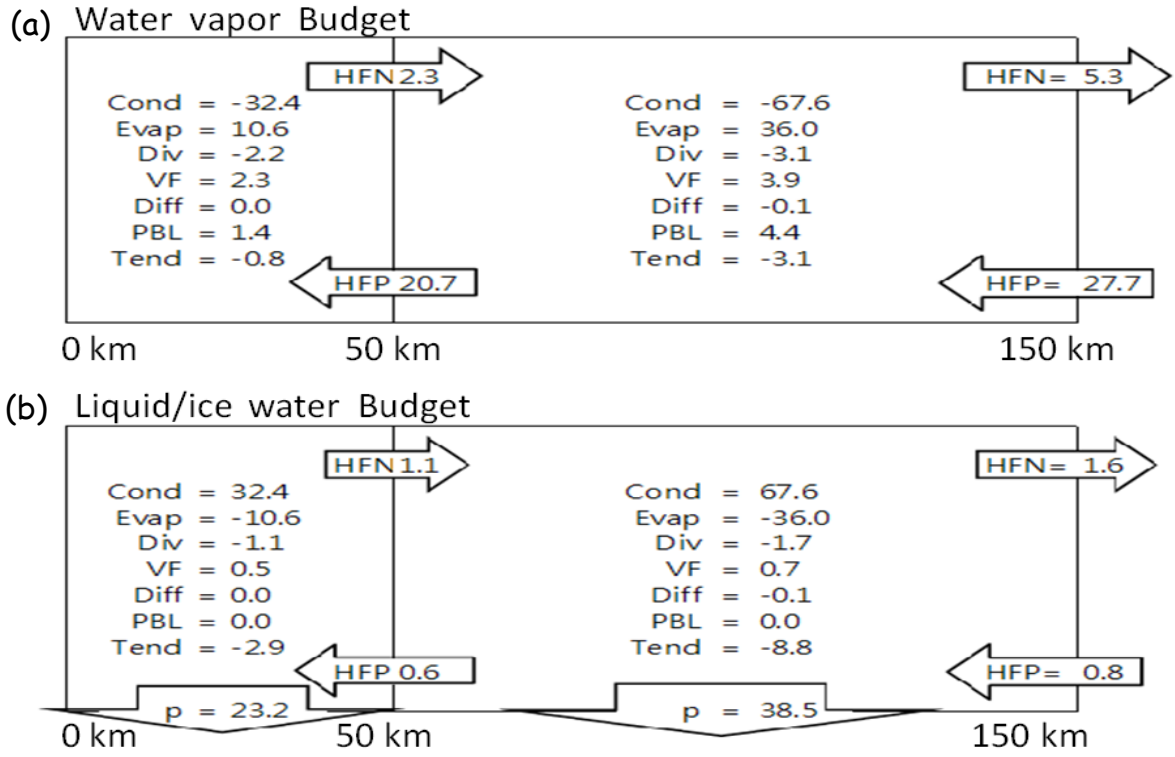

Figure 5: (a) Water vapor budget and (b) total condensate (cloud plus precipitation) budgets of Typhoon Nari over the ocean. All budget terms are normalized by total condensation within R = 150 km, 6.98 x 10^{11} kg h^{-1}. The left portions of the diagrams represent the inner-core of Nari (eye and eyeall, R < 50 km), and the right portions are for the outer rain-band region (50 km < R < 150 km). Parameter names for budget terms are provided in Table 1.

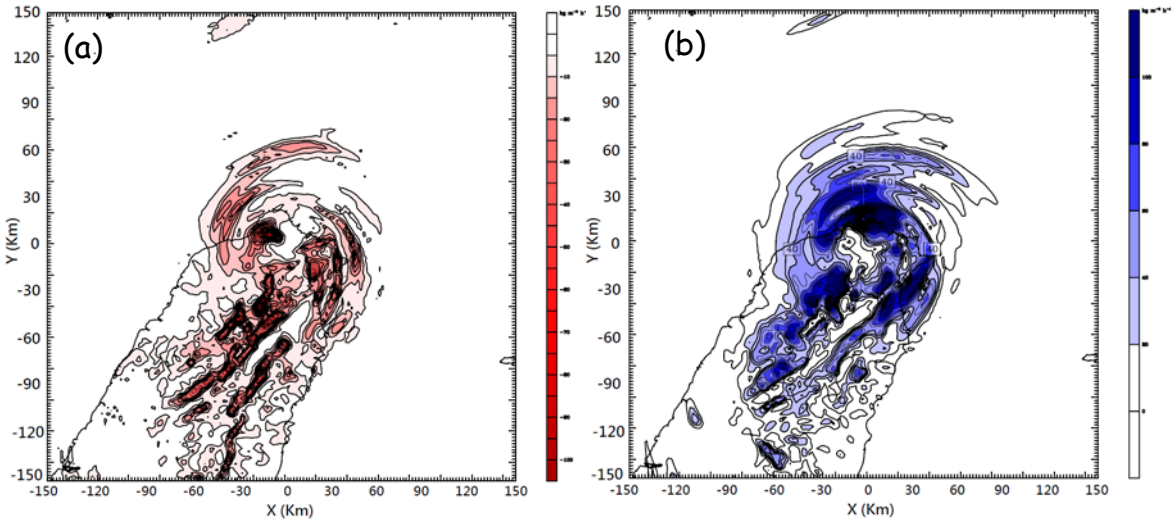

Figure 6: As in Fig. 2 but for the volume integral of one-hour (23–24 h) temporal averaged microphysical source terms of (a) evaporation and (b) condensation. Contour intervals are 5 kg m^{-2} h^{-1} in (a) and 10 kg m^{-2} h^{-1}in (b).